Available online at www.sciencedirect.com
ScienceDirect
Trans. Nonferrous Met. Soc. China 26(2016) 51−62
Transactions of Nonferrous Metals Society of China
www.tnmsc.cn

# Characterization of dynamic microstructural evolution of AA7150 aluminum alloy at high strain rate during hot deformation

Fu-lin JIANG[1,2], Hui ZHANG[1,3], Shu-chu WENG[1], Ding-fa FU[1,3]

1. College of Materials Science and Engineering, Hunan University, Changsha 410082, China;
2. Department of Materials Science and Engineering, McMaster University, 1280 Main Street West, Hamiltion, Ontario L8S 4L7, Canada;
3. Hunan Province Key Laboratory for Spray Deposition Technology and Application, Hunan University, Changsha 410082, China

Received 14 January 2015; accepted 2 June 2015

**Abstract:** The AA7150 aluminum alloy was compressed to various strains at strain rate of 10 $s^{-1}$ and temperatures of 300 °C and 450 °C, respectively. Flow stress behavior, substructure evolution, morphology and spatial distribution of precipitates were studied based on differential scanning calorimetry analysis and transmission electron microscope observation. The results showed that dynamic flow softening occurs during hot deformation. The main softening mechanism could be concluded as dynamic recovery at 300 °C and continuous dynamic recrystallization at 450 °C. The clear heterogeneous spatial distributions of precipitates are found during deformation and enhanced with increased strain. Higher contents of Cu in *T* phases are found at 450 °C than at 300 °C, which present a transformation process from *T* phases to *S* phases as well. The associated evidence of dynamic precipitation on dislocations and particle-stimulated nucleation, as well as the detailed microstructural inherited relationship and morphological texture (particles preferred orientation) were characterized.

**Key words:** Al−Zn−Mg alloy; hot compression; dynamic phenomena; microstructure

## 1 Introduction

In hot working operations, the fundamental mechanisms of dynamic restoration, i.e., dynamic recovery and dynamic recrystallization, and the associated solutes and constituent phases, have strong influences on subsequent heat treatment and the final mechanical properties of products [1−3]. For aluminum alloys with high stacking fault energy, dynamic recovery (DRV) is frequently recognized as the main dynamic softening mechanism, which balances the effects of straining and work hardening, and leads to enhanced workability dynamically as well. Workability is defined as the degree of deformation that a material can undergo without cracking and then gain its desirable deformed microstructures at given temperature and strain rate. Improved workability means increasing the processing ability and also improving properties of the products, which can be achieved by utilizing optimum processing parameters. However, numerous difficulties usually arise due to limited knowledge of the exact hot deformation behavior of specific materials with increased additions of various alloy elements (Zn, Mg, Cu, Mn, etc.) under conditions encountered in processing operations, such as extrusion, forging and hot rolling.

Clear understandings of hot deformation behavior of various aluminum alloys were the targets of many researches in recent years [1,4−7]. In most Al−Zn−Mg system alloys, DRV is the main mechanism balancing work hardening, while dynamic precipitation (DPN), especially precipitation coarsening at higher temperature, results in some flow stress dropping during hot deformation as well [2,8]. CERRI et al [2] studied the hot workability of 7012 and 7075 aluminum alloys prepared by different pretreatment methods, i.e., direct chill cast, homogenized and precipitation treated. The results demonstrated that DPN results in very high peak

**Foundation item:** Project (20130161110007) supported by the Doctoral Program of the Ministry of Education, China; Project (CX2013B128) supported by Hunan Provincial Innovation Foundation for Postgraduate, China; Project (201306130021) supported by the Chinese Scholarship Council
**Corresponding author:** Hui ZHANG; Tel: +86-731-88664086; Fax: +86-731-88821483; E-mail: zhanghui63hunu@163.com, zhanghui63@hnu.edu.cn
DOI: 10.1016/S1003-6326(16)64087-6

stress at low temperatures for solution-treated specimens. As a consequence, the activation energy was about 50% higher than that of precipitated alloys. While the ductility of the extruded alloys was much better than the as-cast material due to the refinement and homogeneous distribution of particles. More than two times activation energy of the water-quenched 7050 aluminum alloy than that of the furnace-cooled alloy was also proved [9], and this was explained by DPN and precipitates coarsening during hot deformation. In addition, dynamic recrystallization (DRX) also played a key role in defining the working softening with decreased temperature compensated strain rate, i.e., Zener−Hollomon parameter ($Z$) values [5,10]. JIN et al [5] concluded that dynamic recovery and recrystallization were the main mechanism of flow softening at low $Z$ values. And dynamic precipitation and successive dynamic particles coarsening, enhanced by higher strain energy, were responsible for the flow softening of 7150 aluminum alloy at low deformation temperature and high strain rate. HU et al [10] studied the softening mechanism of the 7050 aluminum alloy and suggested that DRV transformed to continuous dynamic recrystallization (cDRX) with decreasing $Z$ values and played a major role in flow softening.

Al−Zn−Mg−Cu alloys present a wide range of potential structural applications in aerospace and automotive industry due to their specific mechanical properties. AA7150 aluminum alloy was developed with higher fracture toughness, stress corrosion cracking resistance and strength than that of 7050 aluminum alloy, which has attracted certain interest of many researchers in recent years [5,11−14]. In the present work, AA7150 aluminum alloy was compressed to various strains at strain rate of 10 $s^{-1}$ and at temperatures of 300 °C and 450 °C, respectively. Flow stress behavior, substructure evolution, morphology and spatial distribution of the precipitates were studied based on differential scanning calorimetry (DSC) analysis and transmission electron microscope (TEM) observation. This research contributes to better understanding of the flow softening mechanisms and dynamic microstructure evolutions during thermomechanical processing and optimization of manufacturing processes of Al−Zn−Mg−Cu alloys.

## 2 Experimental

The experiments were carried out on a commercial AA7150 aluminum alloy with nominal chemical composition of 6.38% Zn, 2.32% Mg, 2.11% Cu, 0.09% Zr, 0.06% Si, 0.08% Fe, 0.053% Ti and Al balance (mass fraction). The experimental ingots were homogenized at 465 °C for 24 h and then air cooled. Then, the homogenized AA7150 aluminum alloy blocks were machined to cylindrical specimens with 10 mm in diameter and 15 mm in height. The flat ends of the specimen were recessed to a depth of 0.2 mm to entrap the lubricant of graphite mixed with machine oil during compression so that friction on the specimen/die interface could be minimized. Uniaxial isothermal compression tests were carried out on the Gleeble−1500 thermomechanical simulation machine at a strain rate of 10 $s^{-1}$ and deformation temperatures of 300 and 450 °C, respectively. The compression samples marked with $A_1$, $B_1$, $C_1$, $D_1$, $E_1$, at 300 °C and $A_2$, $B_2$, $C_2$, $D_2$ and $E_2$ at 450 °C, response to critical strains of 0 (pretreatment samples), 0.2, 0.4, 0.6 and 0.8, respectively (Fig. 1). The sample is heated to deformation temperature at a heating rate of 10 °C/s and held at that temperature for 5 min by thermocoupled-feedback-controlled AC current before compression. After compression deformation, the specimens were immediately quenched to room temperature by water to reserve the deformed structure. The deformed structures were sectioned parallel to the compression axis along the direction of centerline and prepared by the conventional methods for DSC analysis at a heating rate of 10 °C/min on NETZSCH STA 449C apparatus. The DSC experiments were firstly carried out on a standard high purity aluminum cell to get the referenced baseline. Then, the alloy sample was fixed into the standard cell for the DSC testing. The baseline recorded from the pure Al sample was subsequently subtracted from the alloy scans at the same heating rate (10 °C/min). The mass of disc-shaped alloy sample was 15−25 mg. To avoid oxidation of the samples, thermal scans were carried out with the argon flow rate of ~10 mL/min. TEM observations were carried out on JEOL JEM−3010 transmission electron microscope operated at 300 kV after electropolishing in a solution of 30% $HNO_3$ and 70% methanol at 25 V and at −30 °C.

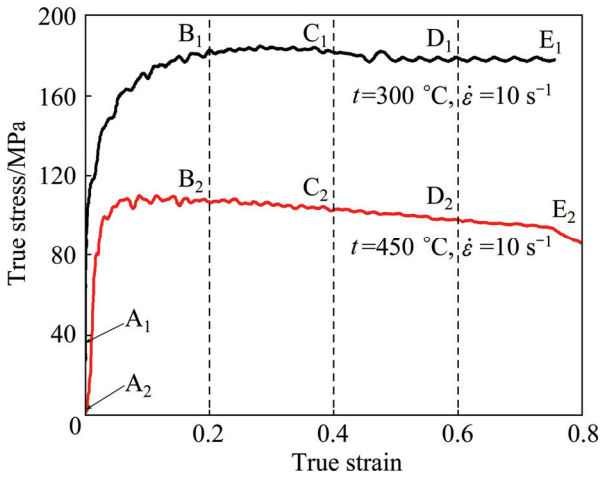


**Fig. 1** True stress−true strain curves of AA7150 aluminum alloy during hot compression deformation

## 3 Results and discussion

### 3.1 Flow stress behavior

Typical true stress−true strain curves of AA7150 aluminum alloy deformed to strain of 0.8 at the strain rate of 10 $s^{-1}$ and temperature of 300 °C and 450 °C are shown in Fig. 1. It can be seen that the flow stresses exhibit initial rapid increasing to peak stresses at critical strains, followed by slight decrease which shows dynamic flow softening. The strain hardening rate and peak stress (183 MPa) at 300 °C are much higher than those at 450 °C (110 MPa), while flow softening seems to be more obvious when deformed at a higher temperature. Flow softening can be caused by deformation heating and microstructural instabilities inside heat-treatable aluminum alloys during hot deformation, such as DRV, DRX and DPN [1,5]. The actual deformation behavior and flow softening mechanisms will be discussed in detail in following sections by DSC analysis and TEM observation on microstructural evolution of AA7150 aluminum alloy specimens deformed to various strains.

### 3.2 Substructure evolution

Figure 2 shows substructure evolution of AA7150 aluminum alloy deformed to different strain degrees based on TEM observation. It can be seen that few dislocations are observed after preheating at 300 °C and 450 °C before compression. When the specimen was deformed to strain of 0.2 at 300 °C, the alloy exhibited high density of dislocations with dislocation tangling and poorly developed cellularity. With increasing strain, the dislocations annihilated and rearranged through climbing and sliding, leading to slight decrease of dislocation density and formation of cell walls ($\varepsilon$=0.4) and transformation from higher energy status to lower energy. As further deformation was carried out ($\varepsilon$=0.6, 0.8), the cell walls started to form substructures (with size of 0.3−2 μm). The grain boundaries became more straight and clearer with lower angle, dislocations density and dislocations energy, which presented typical DRV. As the deformation temperature increased to 450 °C, well developed cell walls formed with size of 0.4−1 μm at strain of 0.2. When the strain increased to 0.4, substructures (with size of 1−4 μm) were well developed, inside which some dislocations and cellularity still existed. With further deformation undergoing ($\varepsilon$=0.6, 0.8), dislocations and cellularity gradually disappeared, and subgrain growth was observed. At the same time, high-angle subgrain boundaries or recrystallized grains gradually formed, while small size and low-angle boundaries subgrains (with size of 0.3−1 μm) could be seen along the boundaries as well.

The growth of dislocation networks can be treated in terms of thermally activated glide, cross-slip, climb and solute drag as rate-controlling mechanisms [15]. Subgrain growth is analogized in a manner that is analogous to normal grain growth with climb of boundary dislocations being the rate controlling

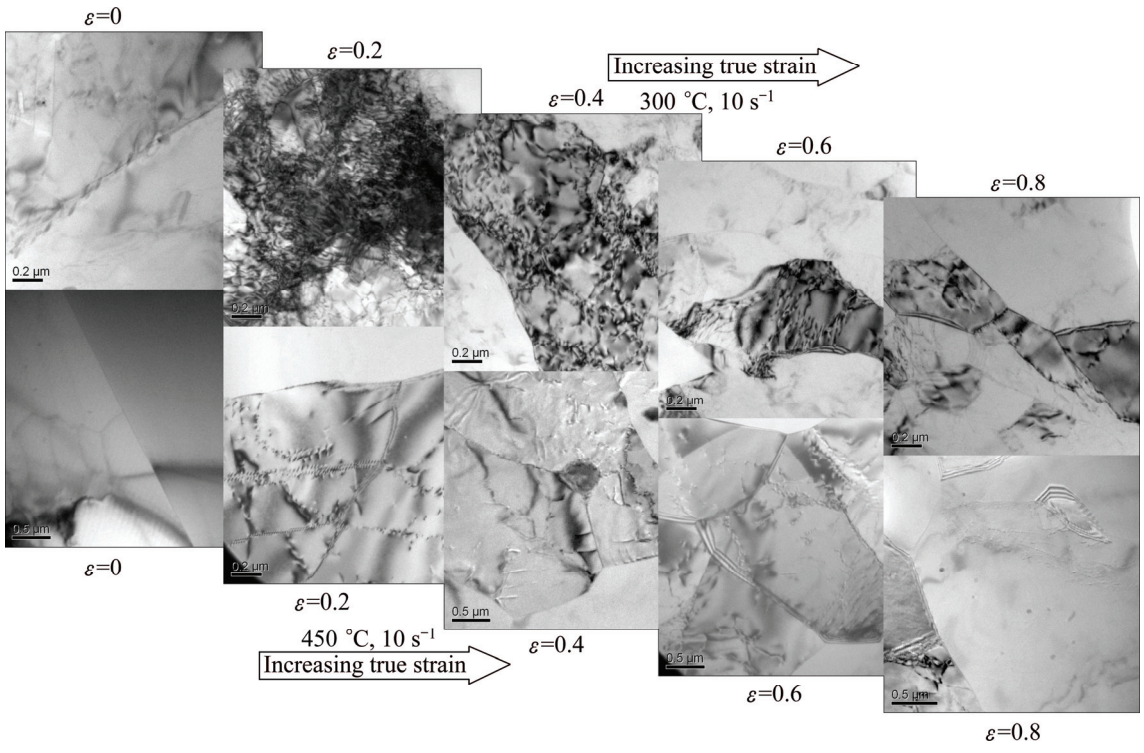


**Fig. 2** TEM images of substructure evolution deformed at different strains and temperatures

mechanism. In general, the alloys deformed at a relatively high strain rate only have very short deformation time before quenching to room temperature. Thus, the deformed microstructure generates a high density of local components with high stored deformation energy instantly, which can act as nucleation sites for new grains or subgrains. The strain rate is relatively high (10 $s^{-1}$) in the present work, and the temperature is too low to increase the mobility of dislocations and grain boundaries when deformed at 300 °C. Hence, the main soften mechanism is DRV at 300 °C [2,8,15]. Such softening decreases the stored energy by dislocation movement and low energy subgrain boundaries formation. When deformed at 450 °C, the high thermal activation energy promotes the mobility of dislocations and grain boundaries, which results in fast formation of cells, subgrains, high-angle subgrain boundaries or recrystallized grains within little incubation time during hot deformation at strain rate of 10 $s^{-1}$, corresponding to previous works that the main softening mechanisms are DRV and cDRX during hot deformation at higher temperature [5−7].

### 3.3 Interaction of constituent phases and local crystallography

#### 3.3.1 DSC analysis

The DSC curves of the as-homogenized AA7150 aluminum alloy and the samples preheated at 300 °C ($A_1$) and 450 °C ($A_2$), are shown in Fig. 3. Several typical features are presented. The effect I corresponds to dissolution of GP zones and the effect II is mainly caused by the formation of $\eta$ precipitate and/or $S$ phase [11,12,16−18]. Since higher solid solution was obtained when held at 450 °C, the endothermic peak (~140 °C, effect I) is more obvious for $A_2$ than other samples. In addition, higher solid solution (less pre-existed precipitates) in Sample $A_2$ compared with the as-homogenized and Samples $A_1$ also lead to precipitation of $\eta$ precipitate and $S$ phase, which is illustrated by the different tendencies (two small exothermic peaks) [16−18]. Those should be an evidence of dissolution of $\eta$ precipitates which precipitate during air cooling after homogenization when pre-heated at 450 °C. Previous researches [19,20] showed that a combination of Cu-bearing $T$ phase and Zn-free $S$ phase survived after homogenizing annealing treatment, which are demonstrated by the different slopes in effect III and the shape endothermic peaks (at ~480 °C of effect IV) in Fig. 3, respectively. When the sample was preheated at 450, $T$ phase was dissolved which led to the small peak in peak III. What's more, transformation from $T$ phase to $S$ phase always happened during high temperature annealing [11,12,20]. When continually heated to higher temperature (above 500 °C), exothermic phenomenon occurs and two endothermic peaks (effect V) also appear. The first endothermic peak is more outstanding for the as-homogenized and 300 °C pretreatment samples which might be caused by melting of $Mg_2Si$ particles. While the second endothermic peak is more highlighted for Samples $A_2$ which might be associated with melting of $Al_7Cu_2Fe$ particles. It was suggested that Fe and Si mainly exist in the form of $Al_7Cu_2Fe$ and $Mg_2Si$ particles, respectively. And these two kinds of particles were basically insoluble and quite stable even at 505−515 °C [11,12]. Thus, coarsening of $Al_7Cu_2Fe$ particles may occur when held at 450 °C according to more outstanding endothermic peak around 550 °C. When the temperature exceeds 550−560 °C, all the DSC curves start to drop dramatically, indicating that melting of the $\alpha$(Al) matrix commences.

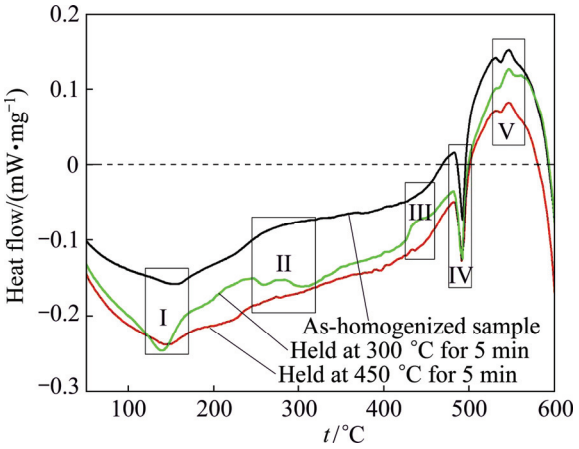


**Fig. 3** DSC curves of AA7150 aluminum alloy samples under various conditions

Previous studies indicated that four major soluble constituent phases, i.e., $\eta$($MgZn_2$), $T$($Al_2Mg_3Zn_3$), $S$($Al_2CuMg$) and $\theta$($Al_2Cu$), can typically exist in Al−Zn−Mg−Cu alloys of commercial interest [11,21]. Two insoluble particles ($Al_7Cu_2Fe$ and $Mg_2Si$) also present in AA7150 aluminum alloy [11,12]. These complex constituent phases, inherited from homogenization process, not only strongly influenced the hot deformation behavior but also affected the final mechanical properties of products [2,22]. Different kinds of particles and their interactions with local crystallography during hot deformation have been characterized in subsequent sections based on TEM observations.

#### 3.3.2 Influence of strain on distribution of constituent phases deformed at 300 °C

DSC analysis indicates that $\eta$ precipitates and $T$ phases are presented during preheating at 300 °C for 5 min prior to deformation. Typical TEM micrographs of $\eta$ precipitates and $T$ phases in the deformed samples are shown in Fig. 4 and Fig. 5, respectively. Numbers of

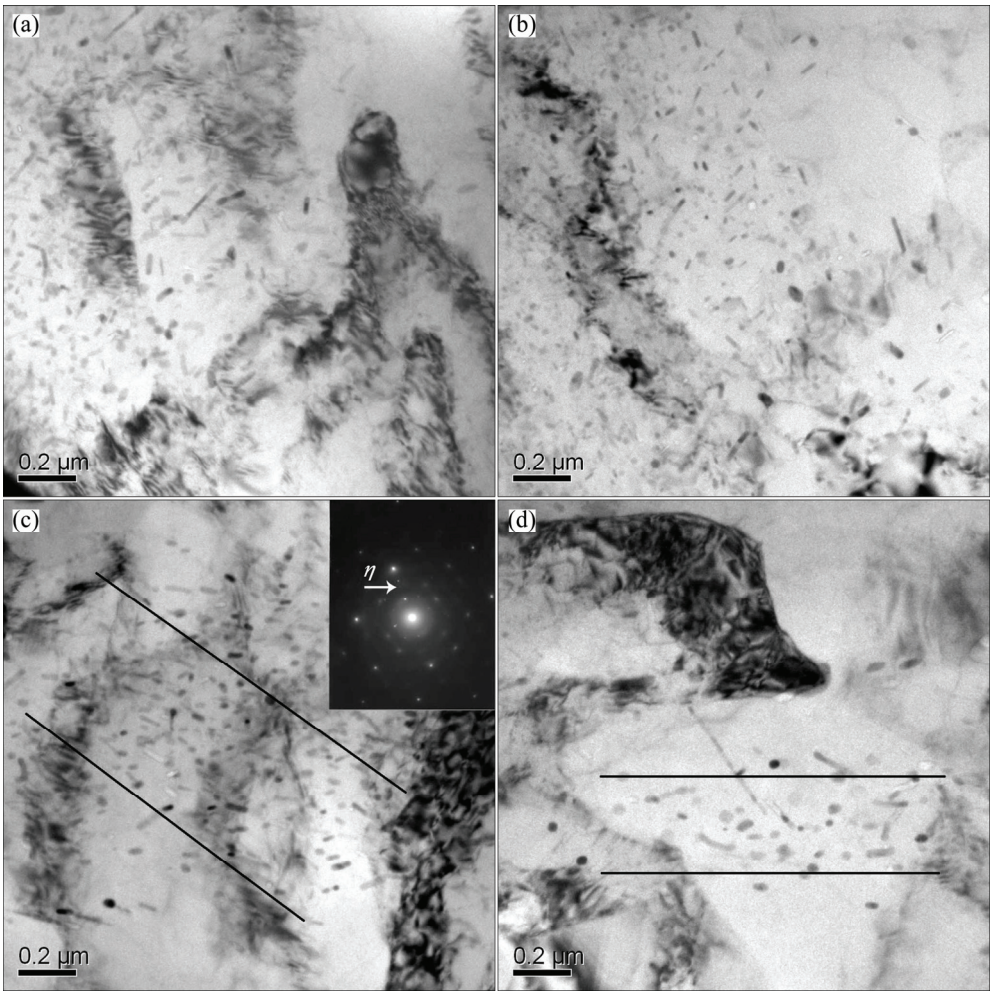


**Fig. 4** Spatial distributions of $\eta$ precipitates deformed at 300 °C under different strains: (a) $\varepsilon$=0.2; (b) $\varepsilon$=0.4; (c) $\varepsilon$=0.6; (d) $\varepsilon$=0.8

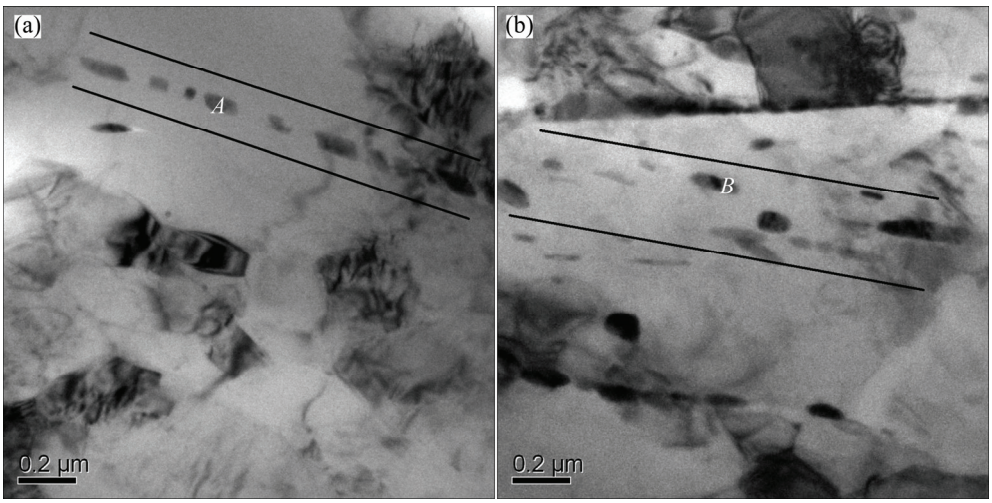


**Fig. 5** Spatial distributions of *T* phases deformed at 300 °C under different strains: (a) $\varepsilon$=0.6; (b) $\varepsilon$=0.8

rod-like $\eta$ precipitates with sizes ranging from 20 to 200 nm were observed clearly when deformed at various strain stages (0.2, 0.4, 0.6 and 0.8). The associated selection area electron diffraction (SAED) pattern of $\eta$ precipitates is shown in Fig. 4(c). At the initial deformation stages ($\varepsilon$=0.2 and 0.4), homogenized distribution of precipitates is shown, while heterogeneous spatial distribution gradually forms when increasing strain to 0.6 or 0.8. In addition, tetragonal or cubic $Al_3Zr$ dispersoids (spherical or bean shaped particles) are presented among $\eta$ precipitates as well, which could provide nucleate sites for $\eta$ precipitates

[23,24]. These heterogeneous spatial distributions or band precipitation, formed during hot deformation, could be a main origin of heterogeneous spatial distribution of $Al_3Zr$ dispersoids after solution treatment, water quenching or aged treatment, which led to heterogeneous $\eta$ precipitates distributed in long and thin bands or even crossed grain boundaries during air quenching and ageing treatment [23−26]. Multiscale-sized particles and precipitates distribution might change markedly throughout processing stages and lead to anisotropy of the final products [2,3,27].

The spatial distribution of *T* phases is also heterogeneous, which are segregated in long and thin bands, and arrayed in lines within the same direction when deformed to strains of 0.6 and 0.8, as shown in Fig. 5. The energy dispersive spectrometer (EDS) analysis results of coarse *T* phases are illustrated in Table 1, which show that small amounts of Cu are still presented in *T* phases.

3.3.3 Influence of strain on distribution of constituent phases deformed at 450 °C

Increased strains also affect the distributions of $Al_3Zr$ dispersoids and coarse *T* phases but few $\eta$ precipitates are observed in deformed specimens at 450 °C. Typical results are given in Fig. 6 and Fig. 7. Most of precipitates could have been dissolved into aluminum matrix after being held at 450 °C for 5 min (Fig. 2) and the process could be accelerated by straining later.

**Table 1** EDS results of soluble constituent particles (Fig. 5) in AA7150 aluminum alloy (mass fraction, %)

| Label | Zn | Mg | Cu | Al |
|---|---|---|---|---|
| A | 20.89 | 1.70 | 4.45 | Bal. |
| B | 15.36 | 1.49 | 5.57 | Bal. |

The non-dissolved $Al_3Zr$ dispersoids have been well studied in literatures, which play a key role in promoting heterogeneous precipitation and inhibiting recrystallization [19,22,25]. The crystallography equilibrium structure of $Al_3Zr$ dispersoids is tetragonal, which are generally observed in their cubic L12 structure and show a very small misfit with the aluminum matrix ($a$=4.08 Å misfit close to 1%) [25]. Numbers of $Al_3Zr$ dispersoids can be easily observed in Fig. 6, which approximate

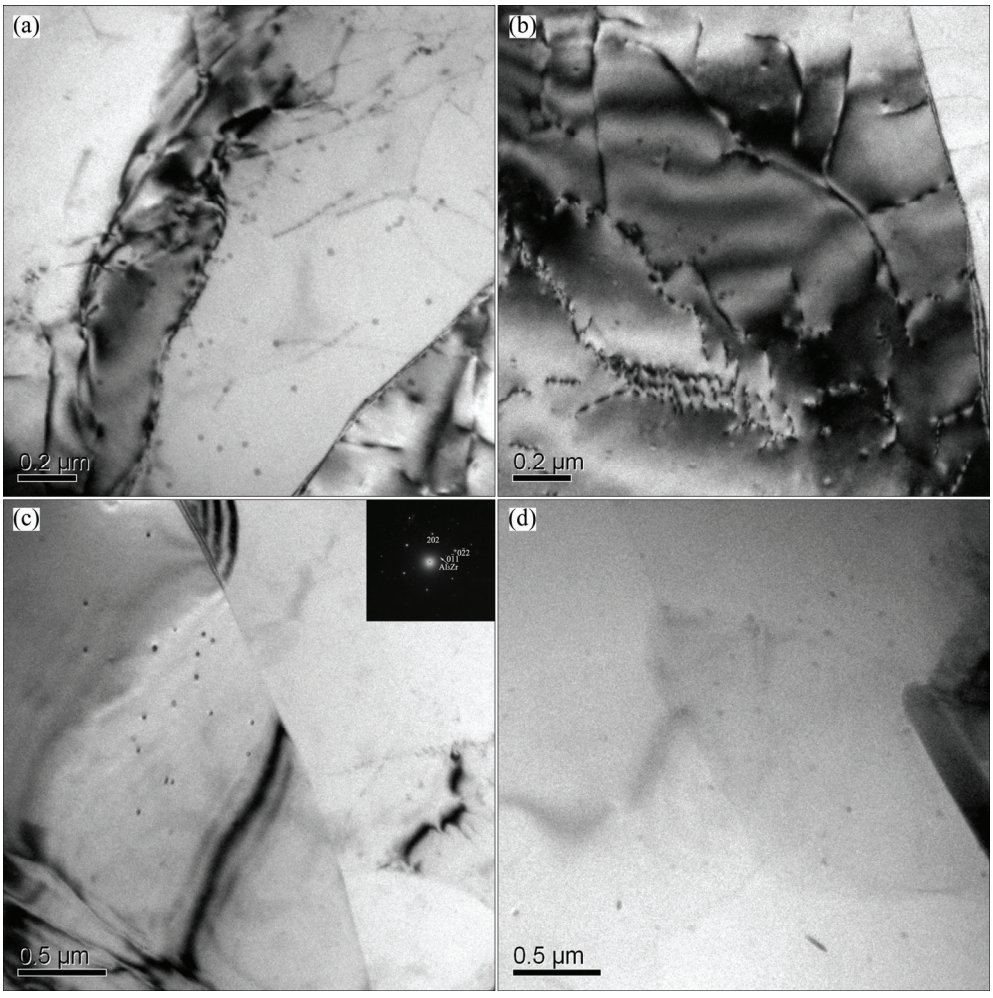


**Fig. 6** Spatial distributions of $Al_3Zr$ dispersoids deformed at 450 °C under different strains: (a) $\varepsilon$=0.2; (b) $\varepsilon$=0.4; (c) $\varepsilon$=0.6 with SAED along $\langle 111\rangle_{Al}$; (d) $\varepsilon$=0.8

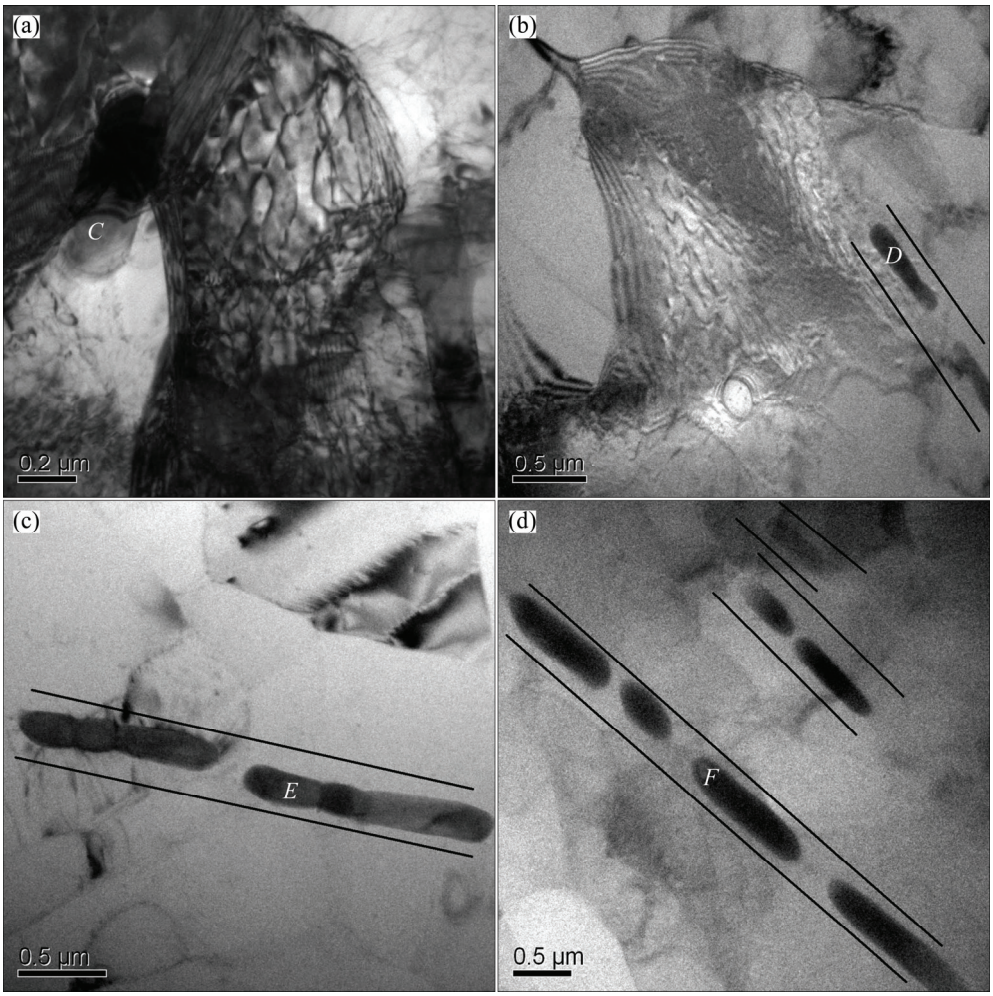


**Fig. 7** Spatial distributions of *T* phases deformed at 450 °C under different strains: (a) $\varepsilon$=0.2; (b) $\varepsilon$=0.4; (c) $\varepsilon$=0.6; (d) $\varepsilon$=0.8

10−30 nm in diameter and are all in epitaxial orientation with the matrix ($\{100\}_{Al_3Zr}//\{100\}_{Al}$) regardless of the grain orientation [21,22,25]. The SAED pattern of $Al_3Zr$ dispersoids was given on the top right corner in Fig. 6(c), which give the relation of $[\bar{1}\,11]_{Al}//[\bar{1}\,11]_{Al_3Zr}$ [25]. Given their small size and low misfit, these mean that $Al_3Zr$ probably totally or partially coherent with aluminum matrix. And the low energy of coherent interface leads to efficient heterogeneous nucleation sites of $\eta$ precipitations during quenching and aging processes [24,25]. The role of $Al_3Zr$ dispersoids in inhibiting recrystallization can be demonstrated that dislocations and subgrains are efficiently pinned by the dispersoids (Figs. 6(a) and (b)) at low strain level. In addition, the spatial distribution of $Al_3Zr$ dispersoids is relatively heterogeneous (Fig. 6), which can be explained by the peritectic nature of the reaction forming $Al_3Zr$ dispersoids and the very low diffusivity of zirconium in aluminum matrix. The peritectic nature causes it to be segregated at the dendrite cores when $Al_3Zr$ precipitates during solidification process. The low diffusivity is responsible for retaining memory of this segregation during subsequent processes [19,22,28].

Generally, the $Al_3Zr$ dispersoids have a strong pining effect during plastic deformation and then inhibit recrystallization [22,25]. Segregated long and thin bands spatial distribution of $Al_3Zr$ dispersoids were observed in quenched thick sheets by DESCHAMPS and BRECHET [25]. Such heterogeneous distribution might root in enhanced heterogeneous distribution of $Al_3Zr$ dispersoids with strain (Fig. 6) during deformation because of very low diffusivity of zirconium in aluminum. Such bands of $Al_3Zr$ dispersoids might lead to bands of $\eta$ precipitates during air quenching [23,24] or overaging procedure [26], because $\eta$ phase preferentially nucleates on dispersoids at high temperatures [23,24]. During subsequent solution treatment, $Al_3Zr$ dispersoids would still exist in bands due to its low diffusivity. Vacancy and higher solid solubility at or around the initial sites of $\eta$ precipitates still remained without enough diffused time as well owing to shorter time in general solution treatment [11,12]. After that $\eta$ precipitates could re-precipitate at the primary sites with low cooling rate or held at high temperature [23,25,26].

Figure 7 shows the distribution status and evolution of *T* phases for AA7150 aluminum alloy samples deformed to different strain degrees at 450 °C. It is obviously observed that the rod-like *T* particles, with diameters and lengths varied between 0.1−0.3 μm and 0.5−1 μm, respectively, are coarser than that deformed at 300 °C. When increasing strain from 0.2 to 0.8, long and thin bands of *T* phases gradually formed and they arrayed in lines in vertical compression direction. The EDS results (Table 2) show that high contents of Cu are presented when deformed at 450 °C. As a matter of fact, the Cu content in the macroscopic *T* phase is much smaller than that at lower temperature [29]. The diffusion velocity of main elements is in the order of Zn>Mg>Cu, with the diffusion constants in Al matrix approximately $4\times10^{-20}$ $m^2/s$ for Zn, $3\times10^{-20}$ $m^2/s$ for Mg, and $0.1\times10^{-20}$ $m^2/s$ for Cu. The homogenization temperature to eliminate the main elements segregation is in the order of Cu>Mg>Zn [29,30]. The slow diffusivity of Cu explains the progressive increase of Cu content when the temperature rises. Therefore, *T* phase could transform to *S* phase during hot compression at high temperature (particle *F* in Table 2).

**Table 2** EDS results of soluble constituent particles (Fig. 7) in AA7150 aluminum alloy (mass fraction, %)

| Label | Zn | Mg | Cu | Al |
|---|---|---|---|---|
| *C* | 44.78 | 3.63 | 26.80 | Bal. |
| *D* | 34.19 | 2.98 | 20.25 | Bal. |
| *E* | 41.13 | 4.18 | 25.13 | Bal. |
| *F* | 22.25 | 2.46 | 49.94 | Bal. |

Heterogeneous and isolated bands of precipitation were demonstrated during quenching and ageing processing, because porosity and vacancies at initial precipitate sites and solute concentration around these precipitates still remained, which were thought to be associated with melting of some residual secondary phases, limited diffusion distances and extended deformation [11,12,25]. Therefore, most of the solutes pumped by the formed precipitates forming during quenching and thermomechanical processing come from the immediate surroundings of these precipitates, so that the remaining material was basically unaffected. The coarse *T* particles at higher temperature were strongly arrayed in lines in vertical compression direction.

3.3.4 Dynamic precipitation on dislocation

A clear TEM image of DPN on dislocation is illustrated in Fig. 8(a) when the sample deformed to strain of 0.4 at 300 °C. It can be seen that numbers of fine precipitates are presented on a dislocation line. A relatively clear precipitate-free zone (PFZ) is shown around the dislocation as well. In order to provide clearer morphologic evidence of DPN on dislocation, a higher magnification TEM image is shown in Fig. 8(b). Generally, dislocation and subgrain/grain boundary are preferential nucleate sites for precipitates which have been studied by many researchers [31]. Dislocation is also short-circuit diffusion path for solutes. Then, the interaction between dislocation and solute will result in a solute flux to dislocation, which leads to lower solute fraction for bulk precipitation and further PFZ (Fig. 8). However, little direct morphologic or visible evidences of DPN were obtained. Previous works have indicated that an important and macroscopical feature of DPN was that the stress−strain curves for the solution treated alloy produce a large peak when compared with the precipitated one. And the peak was usually followed by marked flow softening at lower deformation temperature. The reason was generally suggested to be a combined effect of coalescence of the fine particles and precipitation from the solid solution [1,9]. In researches

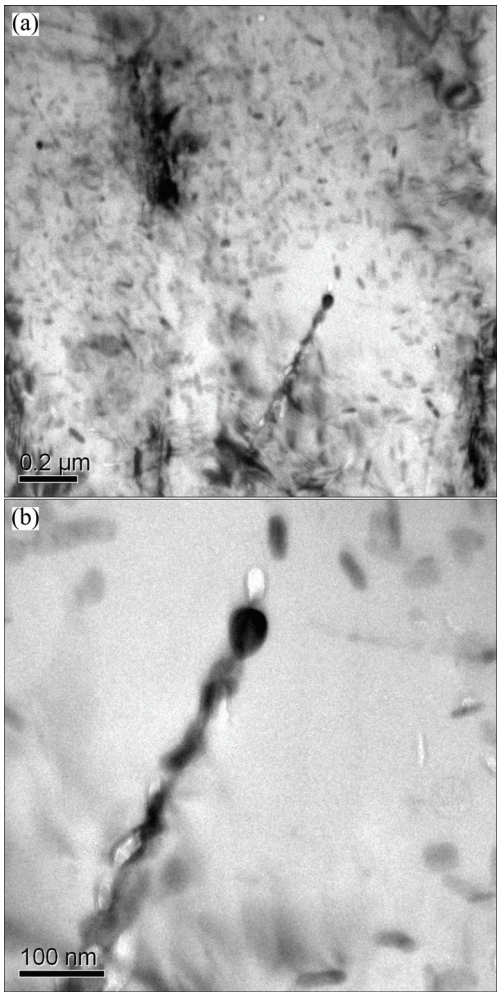


**Fig. 8** TEM image showing direct evidence of dynamic precipitation on dislocation deformed at 300 °C under strain of 0.4 (a), higher magnification TEM image (b) showing previous dynamic precipitation on dislocation

related to controlled rolling of HSLA steels, DPN was observed during hot working of microalloyed steels raising the peak stress and strain. This phenomenon has been confirmed by extraction microscopy, and the rate of DPN was speeded up by a factor of 100 as compared to static precipitation [32]. While for hot deformation behaviors of precipitation hardening aluminum alloys, DPN was initially presented by sharp working softening of flow stress curve, and then lowered the supersaturated solid solubility and resulted in flow softening [1, 2].

3.3.5 Interactions of coarse insoluble constituent phases and local crystallography

The impurity elements of Fe and Si in 7xxx series aluminum alloys mainly existed in the forms of coarse insoluble $Al_7Cu_2Fe$ and $Mg_2Si$ particles, respectively [11,12]. Such coarse particles formed during the initial casting process and could hardly be removed during subsequent processes. Generally, crack initiation and propagation are fostered by the coarse Fe- and Si-rich particles which lead to low fracture toughness. And the residual coarse insoluble particles were found to interact with the dislocations at subgrain boundaries [2]. Figure 9 gives TEM images of interaction between insoluble coarse constituent phases and local crystallography when deformed to different strains at 450 °C. An extra coarse particle, with size of 4−5 μm, is shown in Fig. 9(a). This coarse particle is supposed to be Fe-rich particle ($Al_7Cu_2Fe$) which is analyzed by EDS (Table 3). Around the particle, several high-angle subgrains are well formed. Similar features are presented in Figs. 9(b) and (c) which also contain coarse particles with high-angle subgrains. Such particles are supposed to be Si-rich particles which have alike morphology but different sizes (~0.8 μm in Fig. 9(b) and ~1.2 μm in Fig. 9(c)), as demonstrated by EDS analysis (Table 3).

Large constituent particles imposed local strain heterogeneities and then resulted in high dislocation densities during hot deformation [33,34]. The highly deformed areas around the particles, i.e., the particle affected deformation zones, are effective sites for recrystallization nucleation, particles stimulated nucleation (PSN). These zones contain groups of smaller subgrains with similar orientation and higher density dislocations inside. The nucleation of recrystallization might occur around the coarse particles due to a polygonization process, as shown by HUMPHREYS [33,34]. Typical localized deformation zones, associated with particles larger than about 0.75 μm, acted as preferential nucleation sites for recrystallized grains [2,5,34,35]. JIN et al [5] have found that numbers of fine recrystallization grains appeared around coarse particles based on high magnification optical deformed microstructures at high temperatures. Such recrystallization mechanism could mainly be caused by

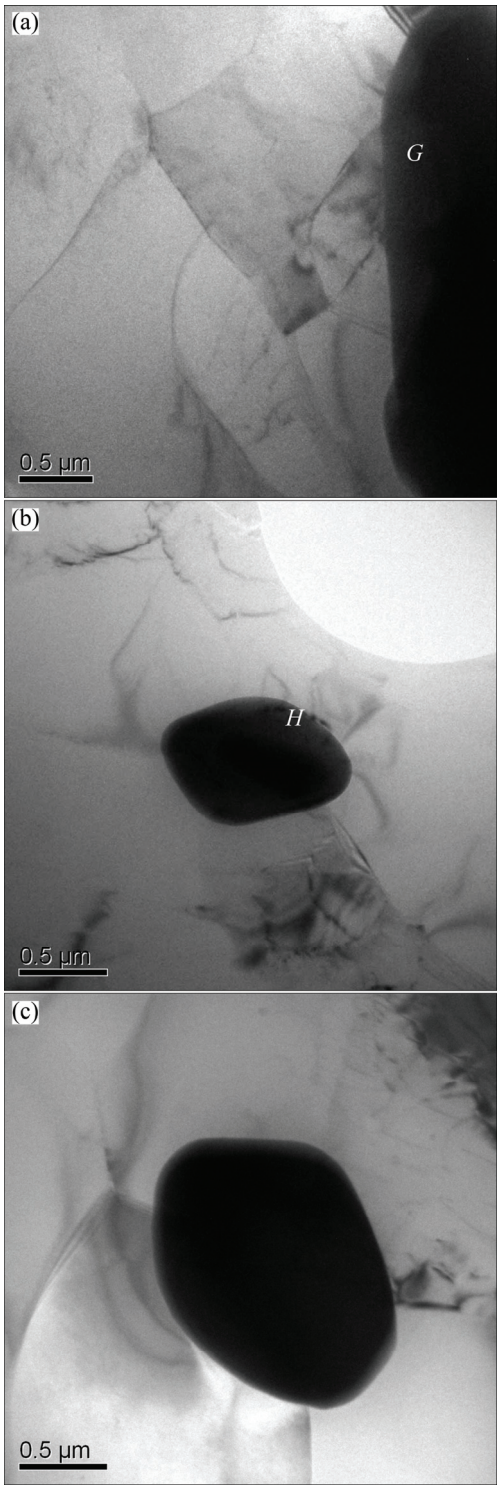


**Fig. 9** TEM images of interactions of insoluble coarse constituent phases and local crystallography deformed at 450 °C under different strains: (a) $\varepsilon$=0.4; (b) $\varepsilon$=0.6; (c) $\varepsilon$=0.8

**Table 3** EDS results of insoluble constituent particles (Fig. 9) in AA7150 aluminum alloy (mass fraction, %)

| Label | Si | Fe | Zn | Cu | Mg | Al |
|---|---|---|---|---|---|---|
| *G* | − | 14.28 | 1.97 | 54.57 | − | Bal. |
| *H* | 85.85 | − | − | 6.79 | 1.83 | Bal. |

strong deformation zones around coarse intergranular particles, which agree well with present TEM observation (Fig. 9). Increasing the volume fraction of coarse particles during pre-ageing can increase the tendency towards an inhomogeneous strain distribution during the subsequent hot work operation, which enhances the possibility of recrystallization during heat treatment [33, 34]. Such methods are always used to gain refinement grains and superplasticity by thermomechanical processing [2,33,35]. On the other hand, coarse particles have a strong effect on recrystallization textures of the worked alloys owing to PSN mechanism [2,36.37].

Insoluble constituent particles, present in the form of $Al_7Cu_2Fe$ and $Mg_2Si$, are found to align in the preferential extension deformation direction during hot working process [3,13,14]. And these particles are found mostly in conjunction with the recrystallized areas, suggesting that recrystallization occurs mainly by PSN mechanism. At the same time, large soluble constituent particles have been found to be elongated along the preferential extension deformation direction as well (Fig. 4, Fig. 5 and Fig. 7) [38]. Based on above discussion, insoluble and soluble particles texture could be summarized to be morphological texture. The insoluble particle texture, existing in particulate reinforced composite as well, will be totally inherited by post-processing and influence the final mechanical property of products, which could be only controlled by cast and forming processing. The soluble particle texture could be partly or completely removed through subsequent heat treatment, for instance improved solution treatment [11,12,39].

## 4 Conclusions

1) Dynamic flow softening occurs with increasing strain during hot deformation of AA7150 aluminum alloy, while higher flow softening is presented at 450 °C than at 300 °C.

2) Typical dislocation tangling and elongated subgrain cellularities developing with increased strain are given at deformation temperature of 300 °C. And faster and larger developed cell walls and subgrains are observed at 450 °C. The main softening mechanism could be concluded as DRV at 300 °C and cDRX at 450 °C due to the presence of high-angle subgrain boundaries.

3) The DSC results show little precipitation when pre-heated at 300 °C, while clear dissolution of precipitates pre-existed when pre-heated at 450 °C. The clear heterogeneous spatial distributions of the presence of $\eta$ precipitates at 300 °C and $Al_3Zr$ dispersoids at 450 °C are found during deformation and enhanced with increased strain. Higher contents of Cu in *T* phases are found at 450 °C than at 300 °C, which present a transformation process from *T* phases to *S* phases as well, and such particles array in line gradually with increased strain during hot deformation.

4) The associated evidence of DPN on dislocations and PSN during hot deformation was presented. The morphological texture, associated with the spatial distribution of constituent particles (soluble and insoluble particles) and the presence of PFZs, gave preferential directions by microstructural inheriting, which might have a strong influence on optimizing processing route and the final mechanical property of products.

## References

[1] McQUEEN H J, KASSNER M E, SPIGARELLI S, EVANGELISTA E. Hot deformation and processing of aluminum alloys [M]. Boca Raton, FL, USA: CRC Press (Taylor & Francis Group), 2011.

[2] CERRI E, EVANGELISTA E, FORCELLESE A, McQUEEN H J. Comparative hot workability of 7012 and 7075 alloys after different pretreatments [J]. Materials Science and Engineering A, 1995, 197: 181−198.

[3] HARNISH S F, PADILLA H A, DANTZIG J A, BEAUDOIN A J, GORE B E, ROBERTSON I M. High-temperature mechanical behavior and hot rolling of AA705X [J]. Metallurgical and Materials Transactions A, 2005, 36: 357−369.

[4] ROFMAN O V, BATE P S. Dynamic grain growth and particle coarsening in Al−3.5Cu [J]. Acta Materialia, 2010, 58: 2527−2534.

[5] JIN Neng-ping, ZHANG Hui, HAN Yi, WU Wen-xiang, CHEN Jiang-hua. Hot deformation behavior of 7150 aluminum alloy during compression at elevated temperature [J]. Materials Characterization, 2009, 60: 530−536.

[6] DENG Ying, YIN Zhi-min, HUANG Ji-wu. Hot deformation behavior and microstructural evolution of homogenized 7050 aluminum alloy during compression at elevated temperature [J]. Materials Science and Engineering A, 2011, 528: 1780−1786.

[7] ROKNI M R, ZAREI-HANZAKI A, ROOSTAEI A A, ABEDI H R. An investigation into the hot deformation characteristics of 7075 aluminum alloy [J]. Materials and Design, 2011, 32: 2339−2344.

[8] DOHERTY R D, HUGHES D A, HUMPHREYS F J, JONAS J J, JENSEN D J, KASSNER M E, KING W E, MCNELLEY T R, McQUEEN H J, ROLLETT A D. Current issues in recrystallization: A review [J]. Materials Science and Engineering A, 1997, 238: 219−274.

[9] LIU Sheng-dan, YOU Jiang-hai, ZHANG Xin-ming, DENG Yun-lai, YUAN Yu-bao. Influence of cooling rate after homogenization on the flow behavior of aluminum alloy 7050 under hot compression [J]. Materials Science and Engineering A, 2010, 527: 1200−1205.

[10] HU H E, ZHEN L, YANG L, SHAO W Z, ZHANG B Y. Deformation behavior and microstructure evolution of 7050 aluminum alloy during high temperature deformation [J]. Materials Science and Engineering A, 2008, 488: 64−71.

[11] XU D K, ROMETSCH P A, BIRBILIS N. Improved solution treatment for an as-rolled Al−Zn−Mg−Cu alloy. Part I. Characterisation of constituent particles and overheating [J].

Materials Science and Engineering A, 2012, 534: 234−243.

[12] XU D K, ROMETSCH P A, BIRBILIS N. Improved solution treatment for an as-rolled Al−Zn−Mg−Cu alloy. Part II. Microstructure and mechanical properties [J]. Materials Science and Engineering A, 2012, 534: 244−252.

[13] CURTIS S A, ROMERO J S, de LOS RIOS E R, RODOPOULOS C A, LEVERS A. Predicting the interfaces between fatigue crack growth regimes in AA7150-T651 aluminium alloy using the fatigue damage map [J]. Materials Science and Engineering A, 2003, 344: 79−85.

[14] ZAIKEN E, RITCHIE R O. On the development of crack closure and the threshold condition for short and long fatigue cracks in AA7150 aluminum alloy [J]. Metallurgical Transactions A, 1985, 16: 1467−1477.

[15] NES E. Recovery revisited [J]. Acta Metallurgica Materialia, 1995, 43(6): 2189−2207.

[16] PARK J K, ARDELL A J. Precipitate microstructure of peak-aged 7075 Al [J]. Scripta Materialia, 1988, 22: 1115−1119.

[17] GHOSH K S, KUMAR A K, MOHAN M K. Calorimetric studies and kinetic parameters of solid state reactions in 7017 Al−Zn−Mg alloy [J]. Trans Indian Inst Met, 2008, 61(6): 487−496.

[18] GHOSH K S, GAO N. Determination of kinetic parameters from calorimetric study of solid state reactions in 7150 Al−Zn−Mg alloy [J]. Transactions of Nonferrous Metals Society of China, 2011, 21(9): 1199−1209.

[19] ROBSON J D. Microstructural evolution in aluminium alloy 7050 during processing [J]. Materials Science and Engineering A, 2004, 382: 112−121.

[20] LIM Seong-taek, LEE Yong-yun, EUN Il-sang. Microstructural evolution during ingot preheat in 7xxx aluminum alloys for thick semiproduct applications [J]. Materials Science Forum, 2006, 519-521: 549−554.

[21] ROKHLIN L L, DOBATKINA T V, BOCHVAR N R, LYSOVA E V. Investigation of phase equilibria in alloys of the Al−Zn−Mg−Cu−Zr−Sc system [J]. Journal of Alloys and Compounds, 2004, 367: 10−16.

[22] WU Ling-mei, WANG Wen-hsiung, HSU Yung-fu, TRONG Shan. Effects of homogenization treatment on recrystallization behavior and dispersoid distribution in an Al−Zn−Mg−Sc−Zr alloy [J]. Journal of Alloys and Compounds, 2008, 456: 163−169.

[23] GODARD D, ARCHAMBAULT P, AEBY-GAUTIER E, LAPASSET G. Precipitation sequences during quenching of the AA 7010 alloy [J]. Acta Materialia, 2002, 50: 2319−2329.

[24] DESCHAMPS A, BRECHET Y. Nature and distribution of quench-induced precipitation in an Al−Zn−Mg−Cu alloy [J]. Scripta Materialia, 1998, 39(11): 1517−1522.

[25] DESCHAMPS A, BRECHET Y. Influence of quench and heating rates on the ageing response of an Al−Zn−Mg−(Zr) alloy [J]. Materials Science and Engineering A, 1998, 251: 200−207.

[26] DUMONT D, DESCHAMPS A, BRECHET Y. On the relationship between microstructure, strength and toughness in AA7050 aluminum alloy [J]. Materials Science and Engineering A, 2003, 356: 326−336.

[27] LIU Sheng-dan, LIU Wen-jun, ZHANG Yong, ZHANG Xin-ming, DENG Yun-lai. Effect of microstructure on the quench sensitivity of AlZnMgCu alloys [J]. Journal of Alloys and Compounds, 2010, 507: 53−61.

[28] MORERE B, MAURICE C, SHAHANI R, DRIVER J. The influence of $Al_3Zr$ dispersoids on the recrystallization of hot-deformed AA 7010 alloys [J]. Metallurgical and Materials Transactions A, 2001, 32: 625−632.

[29] MONDAL C, MUKHOPADHYAY A K. On the nature of T($Al_2Mg_3Zn_3$) and S(Al2CuMg) phases present in as-cast and annealed 7055 aluminum alloy [J]. Materials Science and Engineering A, 2005, 391: 367−376.

[30] MARLAUD T, DESCHAMPS A, BLEY F, LEFEBVRE W, BAROUX B. Influence of alloy composition and heat treatment on precipitate composition in Al−Zn−Mg−Cu alloys [J]. Acta Materialia, 2010, 58: 248−260.

[31] DESCHAMPS A, FRIBOURG G, BRECHET Y, CHEMIN J L, HUTCHINSON C R. In situ evaluation of dynamic precipitation during plastic straining of an Al−Zn−Mg−Cu alloy [J]. Acta Materialia, 2012, 60: 1905−1916.

[32] AKBEN M G, WEISS I, JONAS J J. Dynamic precipitation and solute hardening in AV microalloyed steel and two Nb steels containing high levels of Mn [J]. Acta Metallurgica, 1981, 29: 111−124.

[33] HUMPHREYS F J. The nucleation of recrystallization at second phase particle [J]. Acta Metallurgica, 1977, 25: 1323−1334.

[34] HUMPHREYS F J. Local lattice rotations at second phase particles in deformed metals [J]. Acta Metallurgica, 1979, 257: 1801−1814.

[35] ALARCON O E, NAZAR A M M, MONTEIRO W A. The effect of microstructure on the mechanical behavior and fracture mechanism in a 7050-T76 aluminum alloy [J]. Materials Science and Engineering A, 1991, 138: 275−285.

[36] ENGLER O, KONG X W, LUCKE K. Recrystallisation textures of particle-containing Al−Cu and Al−Mn single crystals [J]. Acta Materialia, 2001, 49: 1701−1715.

[37] BENNETT T A, PETROV R H, KESTENS L A I, ZHUANGD L Z, DE SMET P. The effect of particle-stimulated nucleation on texture banding in an aluminium alloy [J]. Scripta Materialia, 2010, 63: 461−464.

[38] ENGLER O, SACHOT E, EHRSTROM J C, REEVES A, SHAHANI R. Recrystallisation and texture in hot deformed aluminium alloy 7010 thick plates [J]. Materials Science and Technology, 1996, 12: 717−729.

[39] HUMPHREYS F J, MILLER W S, DJAZEB M R. Microstructural development during thermomechanical processing of particulate metal-matrix composites [J]. Materials Science and Technology, 1990, 6: 1157−1166.

# AA7150 铝合金高应变速率热变形过程中显微组织动态演变表征

蒋福林[1,2]，张 辉[1,3]，翁舒楚[1]，傅定发[1,3]

1. 湖南大学 材料科学与工程学院，长沙 410082；
2. Department of Materials Science and Engineering, McMaster University,
1280 Main Street West, Hamiltion, Ontario L8S 4L7, Canada;
3. 湖南大学 湖南省喷射沉积技术及应用重点实验室，长沙 410082

**摘 要**：在温度分别为 300 °C 和 450 °C 条件下对 AA7150 铝合金进行高应变速率(10 $s^{-1}$)热压缩实验。结合差热分析和透射电子显微镜对其不同应变下热变形过程流变行为、亚结构演变及析出相形貌和空间分布进行了系统研究。研究结果表明：AA7150 铝合金热变形过程发生了流变软化，在 300 °C 条件下主要软化机制是动态回复，而 450 °C 条件下为连续动态再结晶；合金热变形过程中 $\eta$ 相(300 °C)及 $Al_3Zr$ 粒子(450 °C)随应变的增加分布不均匀；$T$ 相中的铜含量随温度升高而增加且有从 $T$ 相向 $S$ 相转变的趋势，且随变形量的增加逐渐呈线性排列；显微组织还显示了动态析出及粒子诱发形核再结晶直接相关的形貌特征。

**关键词**：Al−Zn−Mg 合金；热压缩；动态现象；显微组织

**(Edited by Yun-bin HE)**